USE OF SPLIT SPREAD CONFIGURATION OF MARINE MULTICHANNEL SEISMIC DATA IN FULL WAVEFORM INVERSION, KRISHNA-GODAVARI BASIN, INDIA

MAHESWAR OJHA[1], MRINAL K. SEN[2] and KALACHAND SAIN[1]

[1] *CSIR-National Geophysical Research Institute, Hyderabad, India.*
maheswar_ojha@ngri.res.in
[2] *The University of Texas at Austin, Austin, TX 78758, U.S.A.*

(Received January, 27, 2016; revised version accepted April 6, 2016)

ABSTRACT

Ojha, M., Sen, M.K. and Sain, K., 2016. Use of split spread configuration of marine multichannel seismic data in full waveform inversion, Krishna-Godavari basin, India. *Journal of Seismic Exploration*, 25: 359-373.

Estimation of hydrate saturation from seismic reflection data is the primary goal of a gas hydrate exploration program. This requires higher resolution velocity models than can be obtained from standard traveltime tomography. Here, we employ an acoustic full waveform inversion (FWI) in frequency domain with a fixed background density to resolve for fine scale velocity structure of gas hydrate bearing sediments in Krishna Godavari offshore basin of eastern India. Conventional multichannel surface seismic data were acquired in 2010 using 360 channels with 12.5 m receiver interval, 25 m shot spacing and 100 m near offset for the investigation of gas hydrate in this region. We make use of moderate offset conventional end-on multichannel seismic data that are transformed to split spread configuration using reciprocity for use in our FWI. Data redundancy in split-spread configuration provides faster convergence and better resolution in our inversion resulting in a geologically meaningful velocity model. We make use of a smoothed interval velocity model derived from root mean square (RMS) velocity as an initial model and carried out inversion for fourteen frequencies in the range of 8 to 21 Hz at 1 Hz interval. Our results demonstrate that the split-spread dataset is able to resolve subsurface features much better than the conventional end-on data. For example, we notice marked improvement in identification of the free gas layer below the hydrate bearing sediments and many structural features like faults are conspicuous in the final image.

KEY WORDS: split-spread marine seismic data, FWI, Krishna Godavari basin, gas hydrate.

0963-0651/16/$5.00

INTRODUCTION

Occurrences of gas hydrates in shallow marine sediments have been reported in several investigations worldwide (Collett et al., 2009). A huge amount of methane gas is believed to be stored as frozen ice in shallow marine sediments when the temperature and pressure conditions are adequate for their formation. Such methane hydrates are viewed as a drilling hazard as well as a future source of energy by nations that do not have adequate conventional hydrocarbon resources. The government of India through the Ministry of Earth Sciences launched a major exploration program in 2000 (see Sain and Gupta, 2012 for a review) under which the CSIR-National Geophysical Research Institute (NGRI) carried out geophysical exploration including conventional multi-channel and ocean bottom seismic experiments. Gas hydrates are identified from seismic data mostly by detecting an anomalous reflector, known as the bottom simulating reflector (BSR), characterized by seismic attributes, like amplitude blanking, attenuation, velocity anomaly, chimneys, gas escape features, pockmarks, and amplitude variations with offset (e.g., Chand and Minshull, 2003; Ojha and Sain, 2009; Dewangan et al., 2014; Jaiswal et al., 2012). Gas hydrate distribution in the sediments offshore India has been evaluated mostly from BSR signatures and seismic velocity and amplitude anomalies obtained from standard velocity analysis including tomography (e.g., Ojha and Sain, 2009; Sain and Gupta, 2012) and most recently by inversion of pre-stack seismic data (Singha et al., 2014; Wang et al., 2014). Seismic inversion results, such as P- and S-wave velocities, impedances are correlated with well logs to calibrate a rock-physics model, which is then used to predict hydrate saturation from seismic attributes everywhere (e.g., Sen 2006). Unlike other previous reports, here we demonstrate applicability of full waveform inversion (FWI) to a marine multi-channel seismic dataset from offshore India to estimate P-wave velocities that are then used to derive hydrate saturation. The theory of full waveform inversion (FWI) was outlined by Tarantola (1984) and demonstrated by Mora (1987, 1988) three decades ago. Since the last decade, the FWI has been gaining increased popularity for estimating velocity models from seismic gathers directly (e.g., Virieux and Operto, 2009; Mora, 1987, 1988; Pratt et al., 1996; Pratt, 1999, 2004). The method involves iterative fitting of seismic traces with full waveform synthetic seismograms by local optimization techniques, which can be carried out either in time or frequency domain. The advantages and shortcomings of the time-domain and frequency domain have been discussed extensively amongst the exploration geophysics community. We do not focus on this debate; neither do we propose any new development in theory. The primary focus is to demonstrate the applicability of a frequency domain FWI (developed by Seiscope, France) to a split spread configuration of marine multi-channel dataset and discuss the relevant results.

In many applications, FWI in frequency domain has been demonstrated to be effective in building accurate velocity models of complex structures (Pratt, 2004; Virieux and Operto, 2009; Tao and Sen, 2013). Frequency domain FWI can build a compact model for a large volume of data using only a few discrete frequencies. It attempts to mitigate non-linearity in the inverse problem by staging over frequency as it proceeds successively from low to high frequencies. Attenuation can be easily implemented using complex velocities in frequency domain. FWI, in general fails to construct realistic velocity structures from limited offset data through iterative process as the seismic wavefield is insensitive to intermediate wavelengths (Virieux and Operto, 2009). This problem becomes worse in presence of noise, lack of low frequencies, low velocity contrast in seabed and absence of sufficiently accurate initial velocity model to implement FWI in real data (Ravaut et al., 2004; Brossier et al., 2010; Delescluse et al., 2011).

In the work reported in this paper, we generated split-spread data from conventional end-on medium offset marine seismic data. Split-spread data increases data redundancy and thus provides additional constraints and helps to obtain improved results with faster convergence. We have applied an acoustic FWI scheme, details of which can be found in Virieux and Operto (2009). The inverse problem is solved by an iterative approach using a classic steepest-descent method. In the least square sense, the residual wavefield is reduced at every iteration by considering the final model from the previous iteration as the initial model for the current iteration. We used fourteen frequencies ranging between 8 to 21 Hz at 1 Hz interval and 12.5 m grid spacing in our model.

In the following, we describe the study area, inversion strategies and the results.

STUDY AREA AND DATA

Conventional multichannel seismic data were acquired in Krishna Godavari (KG) basin, Bay of Bengal, eastern Indian offshore (Fig. 1a) in 2010 for gas hydrate exploration (Sain et al., 2012). The sedimentary sequence recovered in KG basin is basically a single lithostratigraphic unit dominated by unconsolidated nannofossil-rich clay, where the upper few meters consist of low velocity debris flow (Collett et al., 2008). This margin was formed during Late Jurassic and Early Cretaceous time due to rifting between India and the rest of East Gondwanaland (Powell et al., 1988). The Bengal Fan, world's largest sediment accumulation, is mainly the Himalayan sediment deposited by the Ganges-Brahmaputra River system.

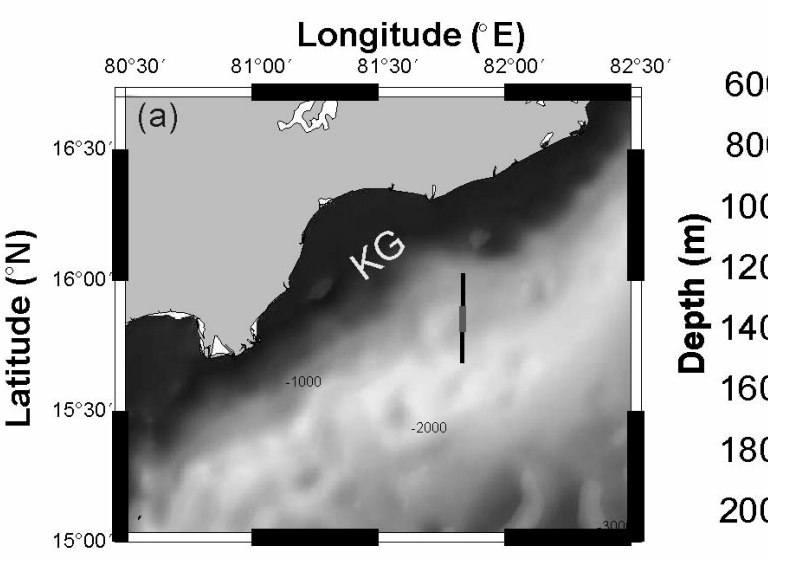

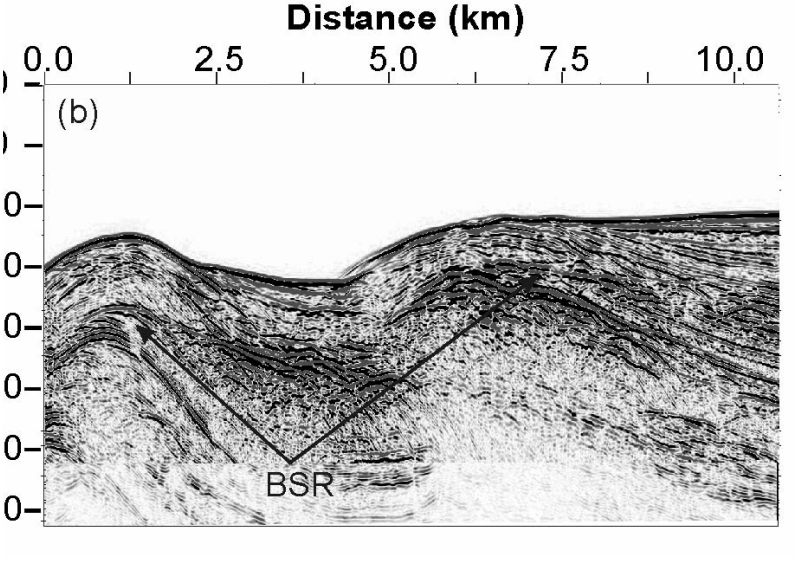

Fig. 1. (a) Location of the study area along with the seismic profile (black line) and bathymetry, and (b) part of the seismic section (along black solid line) used here, showing a bottom simulating reflector. Down headed arrow shows a well location.

Multichannel surface seismic data were acquired using 360 channels with 12.5 m receiver interval, 25 m shot spacing and 100 m near offset (Sain et al., 2012). The data were initially processed using the ProMax software. Due to high swelling noise, we used a bandpass filter with 4-8-24-30 Hz, which restricted us to use a minimum frequency of 8 Hz in inversion. The seismic stack section (Fig. 1b) shows a fairly well demarcated bottom simulating reflector (BSR). The RMS velocity was converted into interval velocity using the Dix's formula. A smoothed version of the interval velocity (Fig. 2a) is used here as an initial velocity model.

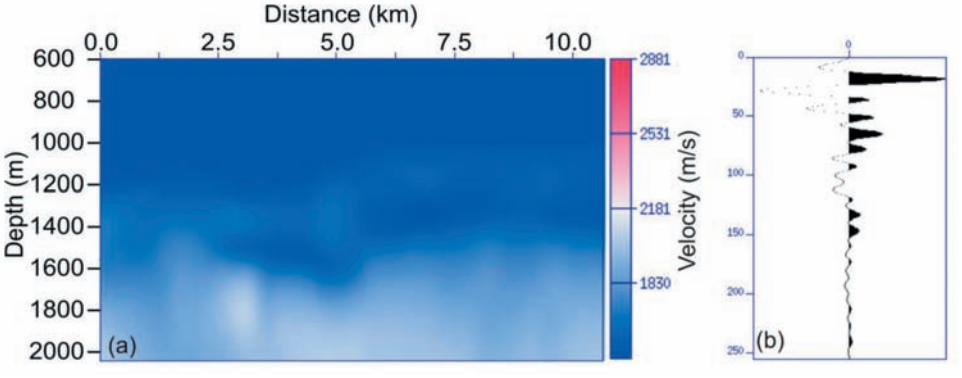

Fig. 2. (a) Interval velocity model derived from the RMS (root mean square) velocity used here as an initial model for inversion and (b) source wavelet used in inversion.

THEORY

As stated earlier, our work reported here focuses on the application of Seiscope's public domain 2D FWI - the details of the theory can be found in Virieux and Operto (2009). We provide below a brief summary, for completeness.

The 2D acoustic full waveform equation in the frequency domain (Marfurt, 1984) is written as

$$\partial^2\mathbf{u}(x,z,\omega)/\partial x^2 + \partial^2\mathbf{u}(x,z,\omega)/\partial y^2 + \omega^2/c^2 = -\mathbf{s}(x,z,\omega) \quad , \qquad (1)$$

where **u** is the seismic wavefield, **s** is source, ω is frequency and c is compressional velocity. Eq. (1) can be rewritten in a linear form as

$$\mathbf{A}\mathbf{u}(x,z,\omega) = \mathbf{s}(x,z,\omega) \quad , \tag{2}$$

where **A** is complex-valued impedance matrix. Eq. (2) is solved here using the mixed-grid finite difference approach (Jo et al., 1996; Stekl and Pratt, 1998; Hustedt et al., 2004) with equal grid spacing. The Perfectly Matched Layers (PML) is used as absorbing boundary conditions (Berenger, 1994). The matrix **A** is factorized by LU decomposition as

$$LU[u1, u2, u3,\ldots\ldots, un] = [s1, s2, s3,\ldots\ldots, sn] \quad . \tag{3}$$

For one source and one frequency, the weighted least-square norm of the cost function used here is given by

$$E(m) = \tfrac{1}{2}\Delta\mathbf{d}^{t}\,\mathbf{W}_{d}\Delta\mathbf{d} \quad , \tag{4}$$

where $\Delta\mathbf{d} = \mathbf{u}_{obs} - \mathbf{u}_{cal}$, is the data misfit vector (difference between observed and synthetic data). Superscript t denotes the transpose conjugate and $\mathbf{W}_d$ is the weighting factor applied to the data that scales the relative contribution of each component of $\Delta\mathbf{d}$. Differentiating eq. (4) with respect to model parameters (m), we get the gradient of misfit function as

$$g_m = \mathrm{Re}(\mathbf{J}^{t}\,\mathbf{W}_{d}\Delta\mathbf{d}^{*}) \quad , \tag{5}$$

where Re denotes real part of a complex value, **J** is the sensitivity or the Fréchet derivative matrix, * denotes the conjugate operator. Eq. (5) can be solved using adjoint-state method (Plessix, 2006) as

$$g'_m = \mathrm{Re}[\mathbf{u}^{t}(\partial\mathbf{A}^{t}/\partial m_i)\mathbf{A}^{-1}\mathbf{W}_{d}\Delta\mathbf{d}^{*}] \quad , \tag{6}$$

Eq. (6) can be considered as a weighted zero-lag convolution between the incident wave field u and the adjoint residual wavefield back propagated from the receiver positions $\mathbf{A}^{-1}\mathbf{W}_{d}\Delta\mathbf{d}^{*}$. For multiple source and frequencies, the misfit function [eq. (4)] and its gradient [eq. (6)] are obtained by summing the contribution of each source and frequency. Model perturbation is written as

$$\Delta\mathbf{m} = -\alpha\mathrm{Re}(\mathbf{J}^{t}\,\mathbf{W}_{d}\Delta\mathbf{d}^{*}) \quad , \tag{7}$$

where α is called the step length, which controls the amplitudes of the perturbations. $\Delta\mathbf{m}$ is discretized on a Cartesian grid with equal spacing h. The updated model is given by

$$\mathbf{m}^{k+1} = \mathbf{m}^{k} + \Delta\mathbf{m} \quad . \tag{8}$$

As FWI is an ill-posed problem, some regularization are applied to the misfit function (Menke, 1984; Tarantola, 1984; Scales et al., 1990) as

$$\Delta \mathbf{m} = -\alpha(\mathrm{diag}\mathbf{H}_a + \varepsilon \mathbf{I})^{-1}\mathbf{G}_m \mathrm{Re}(\mathbf{u}^t\mathbf{J}^t\mathbf{W}_d\Delta \mathbf{d}^*) \quad , \tag{9}$$

where $\mathrm{diag}\mathbf{H}_a = \mathrm{diag}\mathrm{Re}(\mathbf{J}^t\mathbf{W}_d\mathbf{J}^*)$ denotes the diagonal elements of the weighted approximate Hessian $\mathbf{H}_a$ and $\mathbf{G}_m$ is a special smoothing operator. $\mathbf{G}_m$ is a 2D Gaussian spatial filter whose correlation lengths are adapted to the inverted frequency (Ravaut et al., 2004). The diagonal elements are the square product of the source and receiver Green functions (Pratt et al., 1998). The geometrical spreading effects on amplitude of the source and receivers are removed by dividing data residuals by squared amplitude terms. ε is a small parameter.

Using eq. (2), the source function is estimated (Pratt, 1999) as

$$\mathbf{Au} = o\mathbf{s} \quad , \tag{10}$$

where $\mathbf{s}$ is a priori estimate of the source and o is a complex valued scalar, determined at each inverted frequency over all data by least square sense as

$$o = \mathbf{u}_0^t\mathbf{d}^*/\mathbf{u}_0^t\mathbf{p}_0^* = \sum_{i=1}^{N} \mathbf{u}_{0i}\mathbf{d}_i^* \Big/ \sum_{i=1}^{N} \mathbf{u}_{0i}\mathbf{p}_{0i}^* \quad , \tag{11}$$

where $\mathbf{u}_0$ is the wavefield computed for the source $\mathbf{s}$ and N is the total number source-receiver pairs.

DATA ANALYSIS AND RESULTS

Our initial modeling analysis revealed that a constant density of 1.7 g/cc for the shallow sediments provides better amplitude match of the shallow reflections. The source wavelet shown in Fig. 2b was extracted from data by averaging the 1st channel of direct waves for 50 shots. We have used 400 shots for inversion. In case of end-on configuration, we used 180 channels at 25 m interval per shot. We created split-spread data using 180 channels with 25 m interval using reciprocity, so that we have 180 channels on either side with 25m intervals in each split-spread shot gather. We considered fourteen frequencies in the range of 8 to 21 Hz at a 1 Hz interval, and ran inversion for forty iterations at each frequency. Same set of parameters was used in the inversion of end-on and split-spread data.

Fig. 3 shows the variation of root mean square (RMS) errors as a function of iteration for 14 frequencies. RMS errors decay at a faster rate in split-spread configuration (Fig. 3b) than in the end-on dataset (Fig. 3a). It is quite clear that 40 iterations were sufficient as we notice that after 35th iteration the reduction in misfit is very small. Fig. 4 shows a comparison between the synthetic and

observed data for a single frequency. We observe that the field data matches the synthetic data much better in the split spread case than in the end-on case.

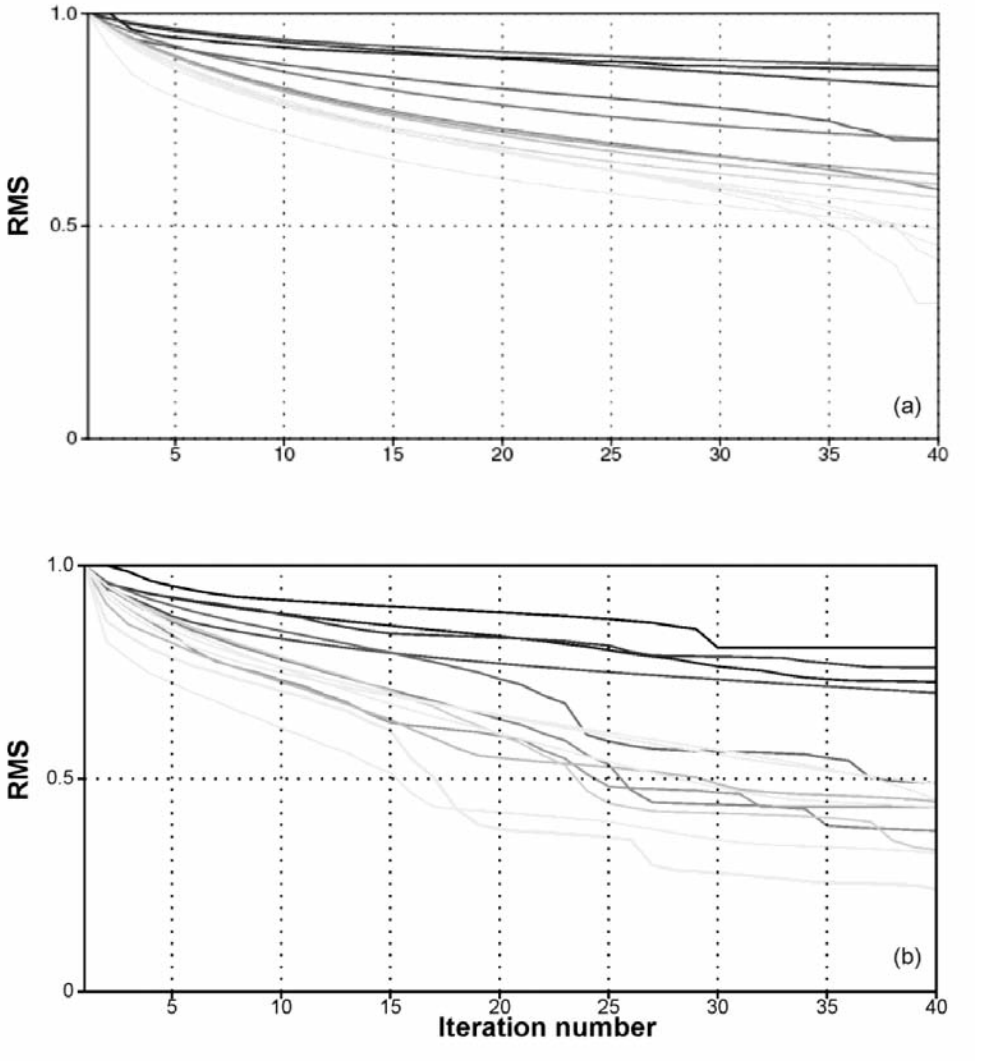

Fig. 3. Root mean square (RMS) error versus iteration for (a) end-on and (b) split spread configuration for 14 frequencies (increasing frequencies from dark to light grey).

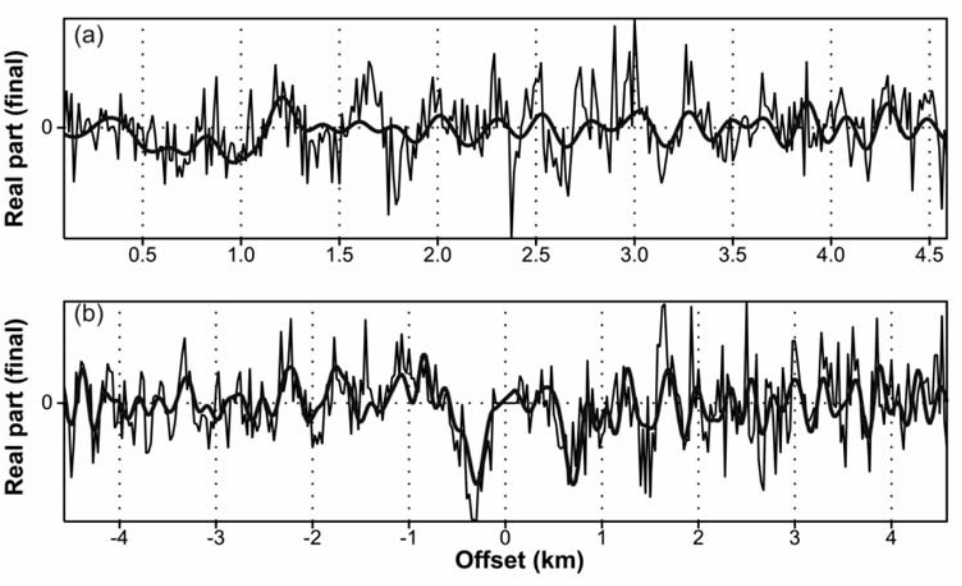

Fig. 4. A comparison of observed (thin lines) and computed (thick lines) seismograms at 1st shot, at 21 Hz frequency and 40th iteration for (a) end-on and (b) split spread configuration.

Fig. 5 shows four inverted velocity models at 15 and 21 Hz after 40th iteration. Models indicate that we need finer grid spacing ($<$ 12.5 m) and higher frequency range to further resolve shallow sedimentary structures with low velocity contrast. Bottom simulating reflector (BSR), which is marked in the seismic section (Fig. 1b) is also visible in Fig. 5d. The results from split-spread configuration (Figs. c-d), show better resolution than those from end-on (Figs. 5a-b). It is clearly visible that closely spaced reflectors and inclined reflectors are well resolved in case of split-spread configuration.

The final velocity-depth function at well location (indicated by arrow in Fig. 1b) is shown in Fig. 6. The initial velocity model (derived from RMS velocity, thin black line in Fig. 6) shows very weak contrast at seabed (maximum 20-50 m/s) and sometimes lower than water velocity due to low velocity debris flow at seabed. Our inverted resulting model clearly resolves the seabed and upper few hundred meters of sediment including the BSR. Although, the velocity derived using split-spread configuration is not exactly matching with sonic velocity, but it shows much closer match than that of the velocity using

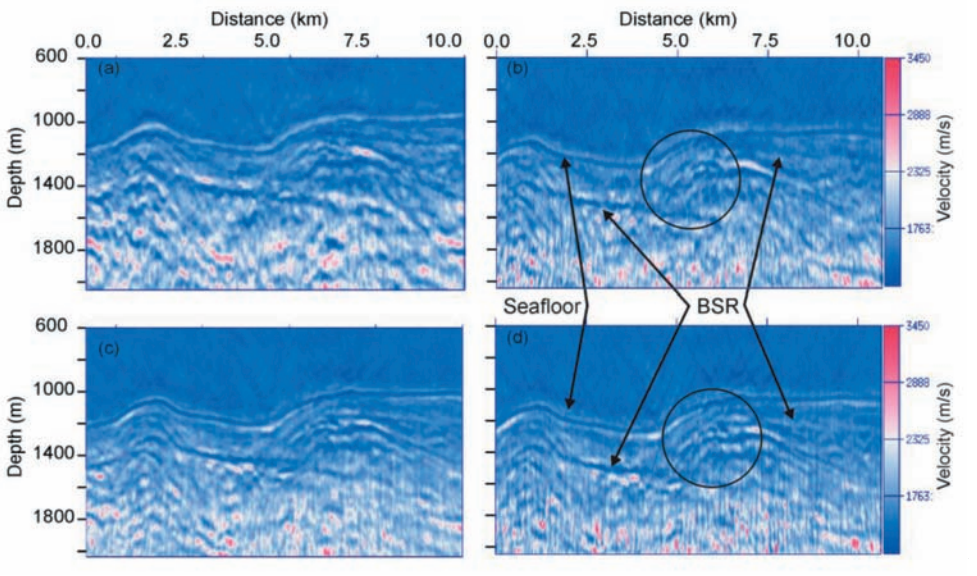

Fig. 5. Inverted velocity models after 40th iteration at frequency 15 Hz (left) and 21 Hz (right), for end-on (a and b) and split-spread configuration (c and d), respectively. Arrow marks and circles show some of better resolved structures in split-spread configuration compared to end-on.

end-on. It is seen that BSR is resolved more distinctly in case of split-spread data. An observed time domain shot gather (Figs. 7a) is compared against synthetic seismic shot gathers generated from the initial (Figs. 7b, c) and the final models (Figs. 7d, e)) for end-on and split-spread confguration, respectively. Synthetic gathers generated from initial and final velocity models show very good convergence of our model. Reflectors are stronger and clear in case of split-spread gather (Fig. 7e) compared to the gather (Fig. 7d) from end-on geometry. It is also seen that the at greater depth, reflectors are resolved better using split-spread configuration compared to the end-on configuration.

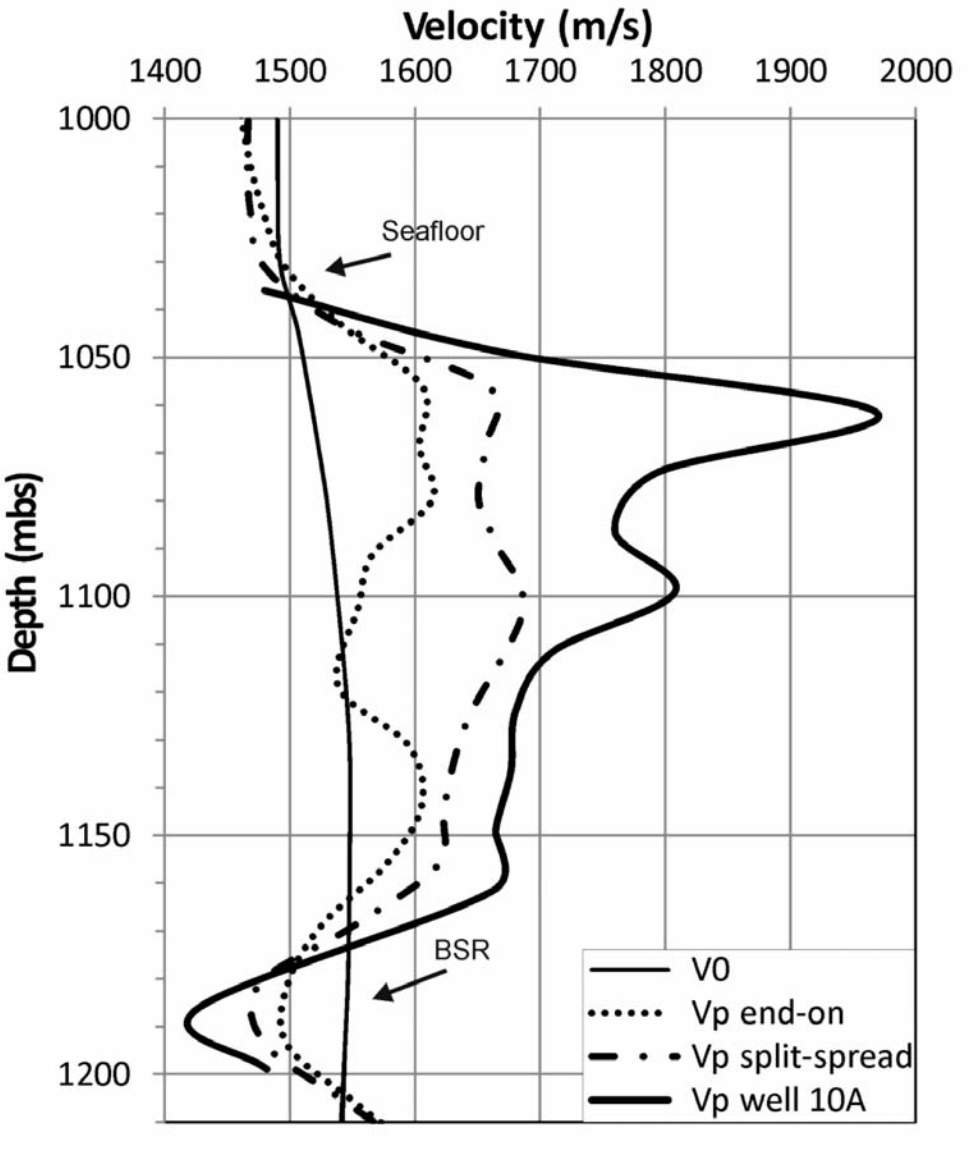

Fig. 6. Inverted velocities (dashed and dotted line) as a function of depth at well location for end-on configuration (dotted line), split-spread configuration (dotted and dashed line), initial velocity (thin solid line) are compared with the sonic velocity (thick solid line).

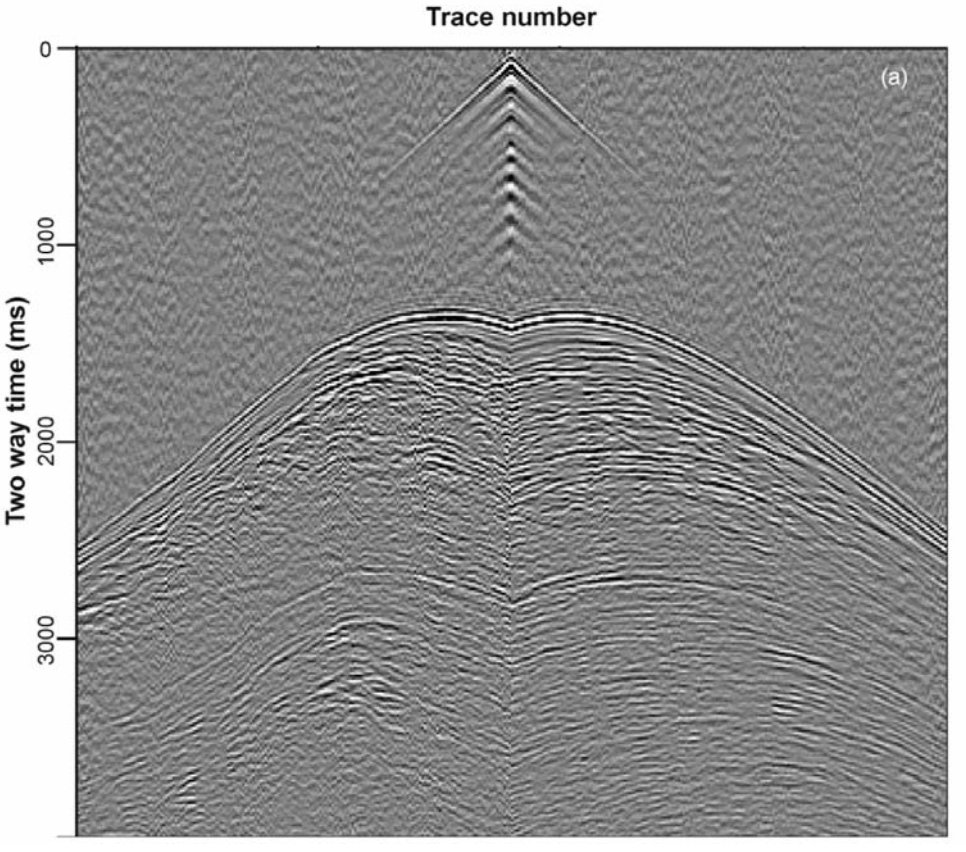

Fig. 7. (a) Observed seismic gather.

DISCUSSION AND CONCLUSIONS

In this paper we have demonstrated the applicability of FWI to estimate a P-wave velocity model of highly porous unconsolidated shallow marine sediment. Unlike other previous studies, we carried out FWI that provided better-resolved velocities, which compare reasonably well with the sonic log at one well location. We found that mapping of the conventional end-on seismic gathers to split spread gathers using reciprocity and their subsequent use in FWI, helped in faster convergence and better resolution of the subsurface structures, especially the complex and dipping strata. One limitation of our approach is the use of an acoustic FWI; use of elastic FWI would provide constraints in shear impedance. We hope to carry out such an analysis in the future. Our study demonstrates that FWI can be a useful tool for estimating velocities of shallow marine sediment and we need further research to optimally implement elastic FWI to real data.

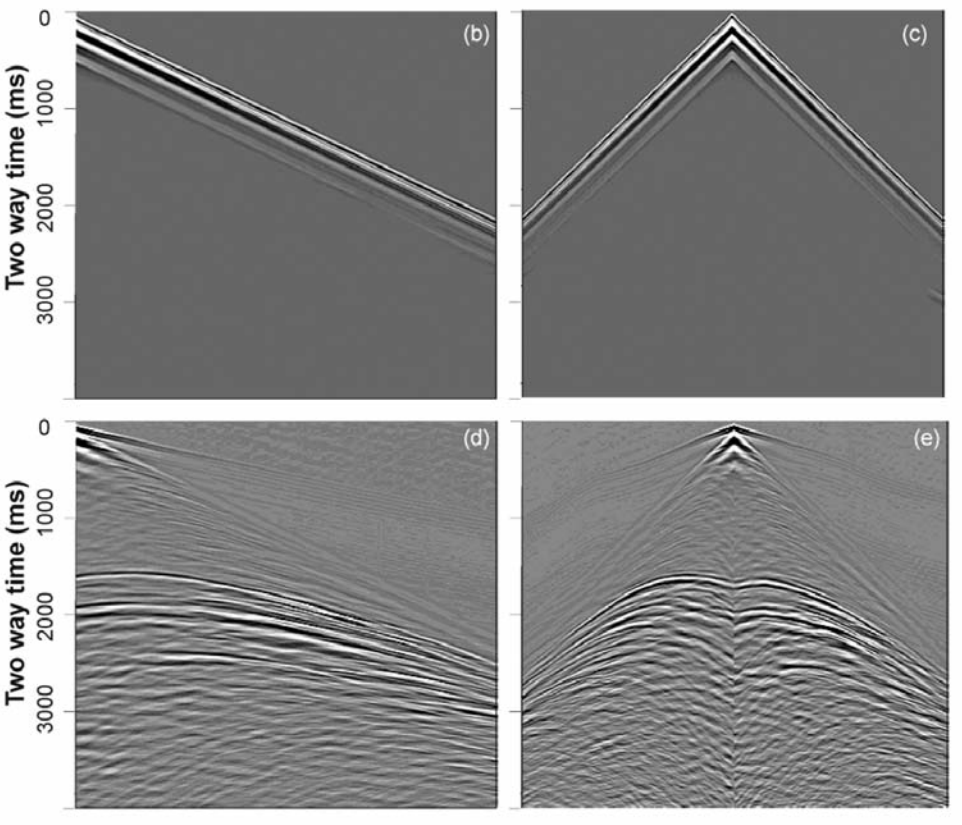

Fig. 7. (b, d) Synthetic seismic gathers using initial and final velocity models for end-on configuration, respectively; (c, e) synthetic seismic gathers using initial and final velocity models for split-spread configuration, respectively.

ACKNOWLEDGEMENTS

The authors are thankful to the director CSIR-NGRI for his kind permission to publish this paper. The Ministry of Earth Science, Delhi is highly acknowledged for financial support to acquire seismic data. Thanks to Yi Tao from UT, Austin for his helping hand to execute the FWI code. This work has been done under CSIR-Shore project. Thanks to SEISCOPE for providing the code and a special thanks to R. Brossier for his kind clarifications of few doubts.

REFERENCES

Berenger, J.P., 1994. A perfectly matched layer for absorption of electromagnetic waves. J. Comput. Phys., 114: 185-200.

Brossier, R., Operto, S. and Virieux, J., 2010. Which data residual norm for robust elastic frequency-domain full waveform inversion? Geophysics, 75: R37-R46.

Chand, S. and Minshull, T.A., 2003. Seismic constraints on the effects of gas hydrate on sediment physical properties and fluid flow: a review. Geofluides, 3: 275-289.

Collett, T.S., Johnson, A.H., Knapp, C.C. and Boswell, R., 2009. Natural gas hydrates: A review. In: Collett, T.S, Johnson, A.H, Knapp, C.C. and Boswell, R. (Eds.), Natural Gas Hydrates - Energy Resource Potential and Associated Geologic Hazards. AAPG Memoir 89: 146-219.

Collett, T., Riedel, M., Cochran, J., Boswell, R., Presley, J., Kumar, P., Sathe, A., Sethi, A., Lall, M. and Sibal, V., 2008. NGHP Expedition 01 Scientists, Indian National Gas hydrate Program Expedition 01 Initial Reports. DGH, India.

Delescluse, M., Nedimovic, M.R. and Louden, K.E., 2011. 2D waveform tomography applied to long-streamer MCS data from the Scotian Slope. Geophysics, 76: B151-B163.

Dewangan, P., Mandal, R., Jaiswal, P., Ramprasad, T. and Sriram, G., 2014. Estimation of seismic attenuation of gas hydrate bearing sediments from multi-channel seismic data: A case study from Krishna-Godavari offshore basin. Mar. Petrol. Geol., 58: 356-367.

Hustedt, B., Operto, S. and Virieux, J., 2004. Mixed-grid and staggered-grid finite difference methods for frequency domain acoustic wave modelling. Geophys. J. Internat., 157: 126-129.

Jaiswal, P., Dewangan, P., Ramprasad, T. and Zelt, C.A., 2012. Seismic characterization of hydrates in faulted, fine-grained sediments of Krishna-Godavari Basin: Full waveform inversion. J. Geophys. Res., 117: B10.

Jo, C.H., Shin, C. and Suh, J.H., 1996. An optimal 9-point, finite-difference, frequency-space 2D scalar extrapolator. Geophysics, 61: 529-537.

Marfurt, K., 1984. Accuracy of finite-difference and finite-elements modeling of the scalar and elastic wave equation. Geophysics, 49: 533-549.

Menke, W., 1984. Geophysical Data Analysis: Discrete Inverse Theory. Academic Press Inc., New York.

Mora, P.R., 1987. Nonlinear two-dimensional elastic inversion of multi-offset seismic data. Geophysics, 52: 1211-1228.

Mora, P.R., 1988. Elastic wavefield inversion of reflection and transmission data. Geophysics, 53: 750-759.

Ojha, M. and Sain, K., 2009. Seismic attributes for identifying gas-hydrates and free-gas zones: application to the Makran accretionary prism. Episodes, 32: 264-270.

Plessix, R.E., 2006. A review of the adjoint-state method for computing the gradient of a functional with geophysical applications. Geophys. J. Int., 167: 495-503.

Powell, C.M., Roots, S.R. and Veevers, J.J., 1988. Pre-breakup continental extension in East Gondwanaland and the early opening of the eastern Indian Ocean. Tectonophysics, 155: 261-183.

Pratt, R.G., 1999. Seismic waveform inversion in the frequency domain, part I: theory and verification in a physic scale model. Geophysics, 64: 888-901.

Pratt, R.G., 2004. Velocity models from frequency-domain waveform tomography: past, present and future. Extended Abstr., 66th EAEG Conf., Paris.

Pratt, R.G., Shin, C. and Hicks, G.J., 1998. Gauss-Newton and full Newton methods in frequency-space seismic waveform inversion. Geophys. J. Internat., 133: 341-362.

Pratt, R.G., Song, Z.M., Williamson, P.R. and Warner, M., 1996. Two-dimensional velocity model from wide-angle seismic data by wavefield inversion. Geophys. J. Internat., 124: 323-340.

Ravaut, C., Operto, S., Improta, L., Virieux, J., Herrero, A. and Dell'Aversana, P., 2004. Multiscale imaging of complex structures from multifold wide-aperture seismic data by frequency-domain full-waveform tomography: application to a thrust belt. Geophys. J. Internat., 159: 1032-1056.

Sain, K. and Gupta, H.K., 2012. Gas hydrates in India: Potential and Development. Gondwana Res., 22: 645-657.

Sain, K., Ojha, M., Nittala, S., Ramadass, G.A., Ramaprasad, T., Das, S.K. and Gupta, H.K., 2012. Gas-hydrates in Krishna-Godavari and Mahanadi Basins: New data. J. Geol. Soc. Ind., 79: 553-556.

Scales, J.A., Docherty, P. and Gersztenkorn, A., 1990. Regularization of nonlinear inverse problems: imaging the near-surface weathering layer. Inverse Probl., 6: 115-131.

Sen, M.K., 2006. Seismic Inversion. Soc. Petrol. Engin., Dallas, TX.

Singha, D.K., Chatterjee, R., Sen, M.K. and Sain, K., 2014. Pore pressure prediction in gas hydrate bearing sediments of Krishna-Godavari basin, India. Mar. Geol., 357: 1-11.

Stekl, I. and Pratt, R.G., 1998. Accurate viscoelastic modeling by frequency domain finite difference using rotated operators. Geophysics, 63: 1779-1794.

Tao, Y. and Sen, M.K., 2013. Frequency-domain full waveform inversion with plane-wave data. Geophysics, 78: R13-R23.

Tarantola, A., 1984. Inversion of seismic reflection data in the acoustic approximation. Geophysics, 49: 1259-1266.

Virieux, J. and Operto, S., 2009. An overview of full waveform inversion in exploration geophysics. Geophysics, 74: WCC127-WCC152.

Wang, J., Sain, K., Wang, X., Nittala, S. and Wu, S., 2014. Characteristics of bottom-simulating reflectors for Hydrate-filled fractured sediments in Krishna-Godavari basin, eastern Indian margin. J. Petrol. Sci. Eng., 122: 515-523.